
Neural Network Compression for Noisy Storage Devices

Berivan Isik¹ Kristy Choi² Xin Zheng¹ Tsachy Weissman¹ Stefano Ermon² H.-S. Philip Wong¹
Armin Alaghi³

Abstract

Compression and efficient storage of neural network (NN) parameters is critical for applications that run on resource-constrained devices. Although NN model compression has made significant progress, there has been considerably less investigation in the actual *physical* storage of NN parameters. Conventionally, model compression and physical storage are decoupled, as digital storage media with error correcting codes (ECCs) provide robust error-free storage. This decoupled approach is inefficient, as it forces the storage to treat each bit of the compressed model equally, and to dedicate the same amount of resources to each bit. We propose a radically different approach that: (i) employs analog memories to maximize the capacity of each memory cell, and (ii) jointly optimizes model compression and physical storage to maximize memory utility. We investigate the challenges of analog storage by studying model storage on phase change memory (PCM) arrays and develop a variety of robust coding strategies for NN model storage. We demonstrate the efficacy of our approach on MNIST, CIFAR-10 and ImageNet datasets for both existing and novel compression methods. Compared to conventional error-free digital storage, our method has the potential to reduce the memory size by one order of magnitude, without significantly compromising the stored model’s accuracy.

to compress and efficiently store the NN parameters. The most commonly used approach is to separate the problem of model compression from physical storage. Reliable digital storage media, fortified by error correcting codes (ECCs), provide error-free storage to users – this allows researchers to develop model compression techniques independently from the precise characteristics of the devices used to store the compressed weights (Bucilua et al., 2006; Cheng et al., 2018). Meanwhile, memory designers strive to create efficient storage by hiding physical details from users.

Although the decoupled approach enables isolated investigation of model compression and simplifies the problem, it misses the opportunity to exploit the full capabilities of the storage device. With no context from data, memory systems dedicate the same amount of resources to each bit of stored information. To address this shortcoming, we investigate the joint optimization of NN model compression and physical storage – specifically, we perform model compression with the additional knowledge of the memory’s physical characteristics. This allows us to dedicate more resources to important bits of data, while relaxing the resources on less valuable bits. Our sole objective is to maximize the storage *density* for a given NN model.

Memory density is of great importance in resource-constrained devices such as mobile phones or augmented reality (AR) glasses. When comparing different memory technologies, density is measured as number of bits stored per silicon area. In this paper, we focus on one memory technology, namely, phase-change memory (PCM), as it is emerging as a compelling alternative to conventional memories. Therefore, density can be simply measured by counting memory cells, and our objective reduces to minimizing the number of memory cells used to store the given model.

To achieve maximum density, we consider the extreme case of analog storage. Recent studies have demonstrated the promise of end-to-end analog memory systems for storing analog data, such as NN weights, as they have the potential to reach higher storage capacities than digital systems with a significantly lower coding complexity (Zarcone et al., 2018; Zheng et al., 2018; Zarcone et al., 2020). However, analog devices are noisy. This has presented several key challenges for the compression task. First, the noise characteristic of

1. Introduction

The rapidly growing size of deep neural networks (NNs) presents new challenges in their storage, computation, and power consumption for resource-constrained devices (Dean et al., 2012; LeCun et al., 2015). This makes it crucial

¹Department of Electrical Engineering, Stanford University, Stanford, US ²Department of Computer Science, Stanford University, Stanford, US ³Facebook, Seattle, US. Correspondence to: Berivan Isik <berivan.isik@stanford.edu>.

such memories is a non-linear function of the input value written onto the cell. Second, slight perturbations of the NN weights from the memory cell may cause the network’s performance to plummet (Achille et al., 2019), which is not accounted for in most NN compression techniques.

Motivated by the above challenges, we draw inspiration from classical information theory and coding theory to develop a framework for encoding and decoding NN parameters to be stored on analog devices (Shannon, 2001). In particular, our method: (i) leverages existing compression techniques such as pruning (Guo et al., 2016; Frankle & Carbin, 2019) and knowledge distillation (KD) (Hinton et al., 2015; Polino et al., 2018; Xie et al., 2020) to learn a compressed representation of the NN weights; and (ii) utilizes various coding strategies to ensure robustness of the compressed network against storage noise.

To the best of our knowledge, this is the first work on NN compression for analog storage devices with *realistic* noise characteristics, unlike previous work that only investigate white Gaussian noise (Upadhyaya et al., 2019; Zhou et al., 2020; Fagbohunge & Qian, 2020). In particular, our contributions are:

1. We develop a variety of strategies to mitigate the effect of noise and preserve the NN performance on PCM storage devices.
2. We present methods to combine these strategies with existing model compression techniques.

Empirically, we evaluate the efficacy of our methods on MNIST, CIFAR-10 and ImageNet datasets and show that storage density can be increased by 16 times on average compared to conventional error-free digital storage.

2. Preliminaries

2.1. Problem Statement and Notation

We consider a supervised learning problem where $x \in \mathcal{X} \subseteq \mathbb{R}^d$ is the input variable, and $y \in \mathcal{Y} = \{1, \dots, k\}$ is the set of corresponding labels. We use capital letters to denote random variables, e.g., X and Y . We assume access to samples $\mathcal{D} = \{(x_i, y_i)\}_{i=1}^n$ drawn from an underlying (unknown) joint distribution $p_{\text{data}}(x, y)$, which are used to train a NN predictor $f_w : \mathcal{X} \rightarrow \mathcal{Y}$. This network, parameterized by the weights $w \in \mathcal{W}$ to be compressed and stored on analog storage devices (where \mathcal{W} denotes the parameter space of NNs), indexes a conditional distribution $p_w(y|x)$ over the labels y given the inputs x .

The NN weights w will be exposed to some input dependent device noise $\epsilon(w)$ when written to the analog storage device, yielding noisy versions of the weights $\hat{w} = w + \epsilon(w)$. In

our experiments, we find that PCM noise dramatically hurts classification performance – as a concrete example, the test accuracy of a ResNet-18 model trained on CIFAR-10 drops from 95.10% (using w) to 10% (using \hat{w}) after the weights are corrupted (via naive storage on analog PCM). Thus to preserve NN performance even after it is stored on the analog device, we explore various strategies $g : \mathcal{W} \rightarrow \mathcal{W}$ for designing *reconstructions* of the perturbed weights $g(\hat{w})$ such that the resulting distribution over the output labels $p_{g(\hat{w})}(y|x)$ is close to that of the original network $p_w(y|x)$.

We note that this notion of “closeness” between the original weights w and the reconstructed weights $g(\hat{w})$ has several interpretations. In Section 3.1.1, we explore hand-designed methods to minimize the distance between w and $g(\hat{w})$ in Euclidean space: $\min_g \|g(\hat{w}) - w\|_2$. In Sections 3.1.2-3.3, we study ways to minimize the Kullback-Leibler (KL) divergence between these two output distributions:

$$\min_g \mathbb{E}_{x \sim p_{\text{data}}(x)} [D_{KL}(p_w(y|x) || p_{g(\hat{w})}(y|x))] \quad (1)$$

where we *learn* the appropriate transformation $g(\cdot)$.

2.2. Phase Change Memory (PCM)

Phase-change memory (PCM) is an emerging memory technology that has the ability to store continuous values (Wong et al., 2010). This makes PCM a compelling choice for future wearable devices. In particular, NN model parameters can be stored in high-density PCM arrays, and thus reducing the total footprint of on-device memories.

As mentioned previously, we only consider PCMs as the main storage for NNs, and aim to reduce the total number of memory cells used for storing a full model. To simulate a realistic storage, we use the PCM model derived from actual measurements collected from experiments on PCM array. Details about the measurements are given in Appendix A. Figure 1 illustrates the PCM model as a *noisy channel*. Each point in Figure 1 corresponds to a possible read (output) value for a given write (input) value. For simplicity, we linearly map both the inputs and outputs to be within range $[-1, 1]$ to satisfy power constraints of the device.

Our realistic PCM model has different noise mean and variance for each input. Using this model is an improvement over prior work that only investigate white Gaussian noise (Upadhyaya et al., 2019; Zhou et al., 2020; Fagbohunge & Qian, 2020) when storing NN models on noisy storage.

Conventionally, memory cells are used to store error-free digital data by allowing enough noise margin between written values. In the case of the model shown in Figure 1, a maximum of 2 bits of data can be stored in each PCM cell. We set this as our baseline: a decoupled approach first does model compression, and then stores the compressed data on a PCM array with the rate of 2 bits per cell. For example,

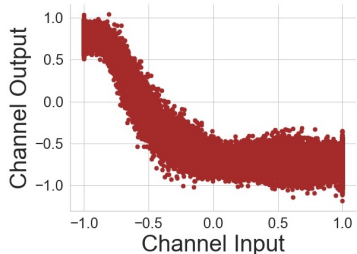


Figure 1. Characteristics of the channel noise in a PCM cell, which is dependent on the input value. Each point corresponds to a possible cell output value for a given input.

1KB of data can be stored reliably on 4,096 PCM cells.

Our method considers using the same PCM cells as analog storage devices. We assume that the read/write circuitry of the PCM has a precision equivalent to that of a single-precision (32-bit) floating point data. This means that a floating point number can be directly written to a memory cell, and the data read back is also a 32-bit float, albeit with the added PCM noise. This simplification allows us to only focus on maximizing memory density, without worrying about read/write circuit complexity. We also assume that random access to model weights are not required, so there will be no “memory packing” problem when storing weights of variable sizes (i.e., different number of cells).

Note that there exists a middle ground between the error-free 2 bit per cell case and the analog storage case. For instance, one can use a PCM cell to store 3 bits of data with some noise. We do not investigate this middle ground and only focus on the extreme case of analog storage, which provides a possible bound for the more practical middle ground.

3. Methodology

3.1. Robust Coding Strategies

In this section, we devise several novel coding strategies for $g(\cdot)$ that can be applied to the model post-training to mitigate the effect of perturbations in the weights. For each strategy, we require a pre-mapping process to remove the non-linearity in the mean of the PCM response in Figure 1.

Inverting the Channel: The mean function of the PCM noise model $\mu : \mathcal{X} \rightarrow \mathbb{R}$ can be learned via a k-nearest neighbor classifier on the channel response measurements as shown in Figure 1. We learn an inverse function $h = \mu^{-1}$ to remove the non-linearity in the mean, since $\phi = C \circ h$ is an identity function with zero-mean noise (Figure 2) where C represents the PCM channel, i.e., $\phi(x) = x + \epsilon_0(x)$ where $\epsilon_0(x)$ is a zero-mean noise with input dependent standard deviation $\sigma(x)$ due to the PCM channel. Thus the relationship between input weights w_{in} to be stored and

output weights w_{out} to be read is:

$$w_{out} = \frac{\phi(\alpha \cdot w_{in} - \beta) + \beta}{\alpha}$$

where α and β are scale and shift factors, respectively. Since the noise is zero-mean, we have:

$$w_{out} = \frac{\alpha \cdot w_{in} - \beta + \epsilon_0(w_{in}) + \beta}{\alpha} = w_{in} + \frac{\epsilon_0(w_{in})}{\alpha}$$

If we use the noisy channel $\phi(\cdot)$ r times (i.e., store the same weight on r “independent” cells and average over the outputs), the relationship between w_{in} and w_{out} becomes:

$$w_{out} = w_{in} + \hat{\epsilon}(w_{in}, r, \alpha)$$

where the standard deviation of $\hat{\epsilon}(w_{in}, r, \alpha)$ is $\frac{\sigma(w_{in})}{\alpha \cdot \sqrt{r}}$ (see Appendix B for the derivation). This provides us two tools to protect the NN weights against zero-mean noise ($\phi(\cdot)$).

(Method #1) Increase the number of channel usage r (increase the number of PCM cells per weight).

(Method #2) Increase the scale factor α under the condition that $\alpha \cdot w_{in}$ satisfies the cell input range limitation ($|\alpha \cdot w_{in} - \beta| \leq 1$).

For the first method, we observe in Figure 2 that the response becomes less noisy as we increase the number of PCM cells used, r . However, we desire to keep r at a minimum for an efficient storage. The second method allows us to make use of the full analog range by scaling the weights. This is particularly useful when storing weights with small magnitude. But we cannot increase α without bound because of the device constraint, that is we need to satisfy $-1 \leq \alpha \cdot w_{in} - \beta \leq 1$ (in practice, this constraint is $-0.65 \leq \alpha \cdot w_{in} - \beta \leq 0.75$ since the remaining portion of the response is non-invertible, and therefore unusable for our purposes). Such limitations leave more to be desired for a general-purpose robust coding strategy for NN weights.

3.1.1. SPARSITY-DRIVEN PROTECTION

Next, we exploit the observation that the weights of a fully-trained NN tend to be sparse (see Appendix C). Table 1 shows that the test accuracy of a Resnet-18 model on CIFAR-10 with weights corrupted by PCM noise drops from 95.10% to 10% (random prediction for CIFAR-10) when less than 64 memory cells are used per weight. If PCM is used as digital storage, 16 PCM cells per weight would be enough since PCM has a capacity of 2 bits and one weight is 32-bit float. Our goal is to preserve classification accuracy by using less than 16 cells per weight to outperform digital storage. (SP+AM+AR) row of Table 1 (the fifth row) shows that we achieve 95.10% accuracy with 3 cells (and 94.44% even

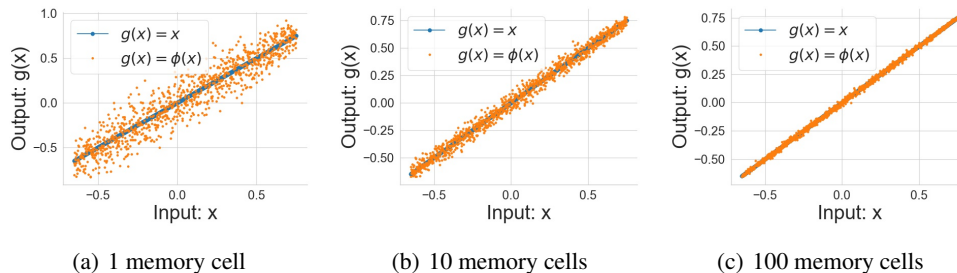


Figure 2. Behavior of $\phi = C \circ f$ (i.e., inverted channel) when outputs are read from an average over 1, 10, 100 cells.

		2056 cells	512 cells	64 cells	32 cells	16 cells	8 cells	4 cells	3 cells	2 cells	1 cell	Additional Bits
ResNet-18 CIFAR-10	No Protection	95.1	94.2	27.1	9.0	10.2	10.2	9.9	9.6	9.8	10.3	0
	SP	95.1	95.0	94.2	94.0	92.8	89.5	67.0	41.9	11.8	9.8	1
	AM+AR	95.0	95.0	94.8	94.7	94.4	93.7	93.1	92.7	89.2	58.0	1
	SP+AM	95.1	95.1	95.0	95.0	94.8	94.7	94.6	93.9	93.2	90.6	2
ResNet-50 ImageNet	SP+AM+AR	95.1	95.1	95.0	95.0	95.0	95.0	95.0	95.1	94.8	94.4	2
	SP+AM+AR+Sens.	95.1	95.1	95.1	95.1	95.1	95.1	95.0	95.1	94.8	95.0	3
	No Protection	67.6	0.001	0.001	0.001	0.001	0.001	0.001	0.001	0.001	0.001	0
	SP	75.6	0.044	0.009	0.001	0.001	0.001	0.001	0.001	0.001	0.001	1
ResNet-50 ImageNet	AM+AR	76.0	75.0	66.7	66.4	63.2	57.5	34.1	22.4	0.037	0.001	1
	SP+AM	76.1	70.6	69.4	55.1	51.3	34.6	28.0	17.6	0.046	0.002	2
	SP+AM+AR	76.6	75.4	74.5	74.2	73.8	73.8	72.8	72.2	70.2	66.0	2
	SP+AM+AR+Sens.	76.6	75.8	75.6	75.3	74.8	74.9	74.5	73.7	73.0	68.8	3

Table 1. Accuracy of ResNet-18 on CIFAR-10 and ResNet-50 on ImageNet when weights are perturbed by the PCM cells. Baseline accuracy (without noise) is 95.1% for CIFAR-10 and 76.6% for ImageNet. SP: sign protection, AM: adaptive mapping, AR: sparsity-driven adaptive redundancy, Sens.: sensitivity-driven adaptive redundancy. Results are averaged over three runs. Higher is better.

with 1 cell) per weight using the sparsity-driven protection; on the other hand, the NN performance is compromised without sparsity-driven protection even using 512 cells per weight with an accuracy of 94.20% (see No Protection row) – more than $512 \times$ times reduction in the required amount of storage. Figure 3 demonstrates the effectiveness of our approach in preserving NN performance on PCM (Figure 6 for CIFAR-10 in Appendix).

Sign Protection: When scaling the weights by α to fit them in range $[-0.65, 0.75]$ of ϕ (Figure 2), small weights are mapped to values very close to zero. This is problematic because a majority of the trained NN weights have small magnitudes, and thus the NN with reconstructed weights will suffer a severe drop in performance due to sign errors (Appendix C). Therefore, we store the sign and magnitude of the weights separately. The sign can be represented by 1 bit and 2 sign bits can be stored using 1 cell. When we store magnitudes instead of actual weights, we can use an α that is twice as large, reducing the variance of noise from Method #2. The (No Protection) and (SP) rows of Table 1 illustrate the effect of sign protection as the required memory to achieve a test accuracy of $94.1 \pm 0.1\%$ on CIFAR-10 is reduced by $16 \times$ times (from 512 cells to 32 cells).

Adaptive Mapping: Although protecting the sign bit leads to accuracy gains on CIFAR-10, we still require more than

16 devices to achieve the original accuracy without PCM noise. To further improve the efficiency, we use the observation that the majority of nonzero weights after pruning are quite small (see Appendix C). This implies that using different values of α depending on the magnitude of the weight (larger scale factor α for small weights) can reduce the overall variance of the cell’s noise from Method #2. This requires an extra bit to indicate whether a weight is small or large since two different α ’s are used in encoding and decoding. Together with the sign bit that we store separately, we need to store 2 bits per weight which can be done using 1 PCM cell per weight. With this strategy, according to (SP) and (SP+AM) rows of Table 1, we can increase the accuracy from 9.8/0.001% to 90.6/51.3% with an average of 1/16 cells per weight on CIFAR-10/ImageNet.

Adaptive Redundancy: Finally, we propose to vary the number of PCM cells used for larger and smaller weights. The average number of cells that we aim to minimize is:

$$r_{avg} = \frac{r_{small} \times N_{small} + r_{large} \times N_{large}}{N_{small} + N_{large}}$$

where N_{small} and N_{large} are the number of small and large weights; r_{small} and r_{large} are the number of cells used per weight for small and large weights, respectively. Using more cells for larger weights (which are more critical for NN performance) increases the accuracy while it does

not increase the average redundancy too much (Method #1) since most weights are sparse, e.g., $N_{small} = 11, 168, 312$ and $N_{large} = 5, 650$ in ResNet-18 trained on CIFAR-10. Sign protection and adaptive mapping help protect mostly the small weights while adaptive redundancy protects large weights by reserving more resources for them. As shown in the (SP+AM) and (SP+AM+AR) rows of Table 1, combining these strategies increases the accuracy by 4%/66% on CIFAR-10/ImageNet for the 1 cell per weight case without requiring any additional bits.

3.1.2. SENSITIVITY-DRIVEN PROTECTION

While we have demonstrated the success of sparsity-driven protection strategies for $g(\cdot)$ even with 1 cell per weight for ResNet-18 on CIFAR-10, the method falls short for more complex datasets. For ImageNet, the accuracy of ResNet-50 with sparsity-driven protection against 1 PCM per weight is 10.6% lower than the original accuracy without PCM noise (76.6%) (see Table 1). To close this gap, we study Eq. 1 in more detail. Let us define δ_w as the final perturbation on the weights, i.e., $g(\hat{w}) = w + \delta_w$. We first approximate the KL divergence via a second-order Taylor expansion:

$$\begin{aligned} \mathbb{E}_{x \sim p_{\text{data}}(x)} [D_{KL}(p_w(y|x) || p_{w+\delta_w}(y|x))] \\ \approx \delta w^T F \delta w + O(\|\delta w\|^3) \end{aligned}$$

where F is the Fisher Information Matrix (Martens, 2014; Grosse & Martens, 2016):

$$F := \mathbb{E}_{x, y \sim p_{\text{data}}(x, y)} [\nabla_w \log p_w(y|x) \nabla_w^T \log p_w(y|x)]$$

Dropping the off-diagonal entries in F yields:

$$\begin{aligned} \delta w^T F \delta w &\approx \mathbb{E}_{x, y \sim p_{\text{data}}(x, y)} \sum_{j=1}^d \left(\delta w_j \cdot \frac{\partial \log p_w(y|x)}{\partial w_j} \right)^2 \\ &= \sum_{j=1}^d \delta w_j^2 \mathbb{E}_{x, y \sim p_{\text{data}}(x, y)} \left(\frac{\partial \log p_w(y|x)}{\partial w_j} \right)^2 \end{aligned}$$

where d is the number of weights. Thus the KL divergence between the conditional distribution parameterized by the original (w) and perturbed weights ($g(\hat{w}) = w + \delta w$) that we aim to minimize is:

$$\begin{aligned} \mathbb{E}_{x \sim p_{\text{data}}(x)} [D_{KL}(p_w(y|x) || p_{w+\delta_w}(y|x))] \\ \approx \frac{1}{N} \sum_{j=1}^d \delta w_j^2 \sum_{i=1}^N \left(\frac{\partial \log p_w(y_i|x_i)}{\partial w_j} \right)^2 \end{aligned}$$

where the expectation is approximated with Monte Carlo samples from the empirical data distribution.

We note that for each weight w_j , we can estimate how much performance degradation a perturbation by δw_j can cause by evaluating the term $\frac{1}{N} \sum_{i=1}^N \left(\frac{\partial \log p_w(y_i|x_i)}{\partial w_j} \right)^2$.

We call this term ‘‘sensitivity’’ and denote it as: $s_j = \frac{1}{N} \sum_{i=1}^N \left(\frac{\partial \log p_w(y_i|x_i)}{\partial w_j} \right)^2$. For the storage of sensitive weights w_j with large s_j , we should use more PCM cells as slight perturbations of these weights may lead to significant changes in the output distributions (Method #1). This will not affect the number of cells per weight on average (r_{avg}) too much because the gradients of a fully trained network is known to be sparse (Appendix C). In fact, $\frac{\partial}{\partial w_j} \log p_w(y_i|x_i)$ is nothing but the Stochastic Gradient Descent (SGD) gradient that is computed at each iteration. Thus ordering the weights based on sensitivity can be done easily with one pass over the whole dataset. In our experiments, we combine sensitivity-driven protection and sparsity-driven protection to vary the number of memory cells per weight according to both magnitude and sensitivity. From (SP+AM+AR) and (SP+AM+AR+Sens.) rows of Table 1, sensitivity-driven protection provides 2.8% improvement in test accuracy using 1 cell per weight for ResNet-50 trained on ImageNet.

Figure 3 illustrates that sparsity-driven and sensitivity-driven protection strategies provide 2056 times more efficient storage of NN models by preserving the accuracy against PCM noise. This makes analog storage for NN weights an appealing alternative to digital storage. We refer the reader to Figure 6 for similar results on CIFAR-10.

3.2. KL Regularization for Robustness

The following set of techniques for constructing $g(\cdot)$ are designed to correct the errors that the robust coding strategies in the previous section fail to address.

3.2.1. ROBUST TRAINING

For robust training, we regularize the standard cross-entropy loss with the KL divergence in Eq. 1. Specifically, the loss function is as follows:

$$\begin{aligned} \mathcal{L}(w) &= \mathbb{E}_{x, y \sim p_{\text{data}}} [-\log p_w(y|x)] \\ &\quad + \lambda \mathbb{E}_x [D_{KL}(p_w(y|x) || p_{g(\hat{w})}(y|x))] \end{aligned}$$

where we approximate the true expectation with Monte Carlo samples from the empirical data distribution. We note that the final perturbation δw on the weights ($g(\hat{w}) = w + \delta w$) can be thought of as a noise or the effect of pruning on the w . In particular, when we apply pruning, we have:

$$\begin{aligned} \delta w_j &= 0 && \text{for a non-pruned weight } w_j, \\ \delta w_j &= -w_j && \text{for a pruned weight } w_j. \end{aligned}$$

In our experiments, we add Gaussian noise as a perturbation δw (i.e., $g(\hat{w}) = w + \delta w$ is a noisy weight), during robust training with the hope that trained network will learn $g(\cdot)$ to be more robust to both PCM and Gaussian noise. We observe that the trained network is also more robust to

pruning in addition to noise. In the magnitude pruning, only the small weights are set to zero, that is δw_j is equal to 0 (for large weights) or $-w_j$ (for small weights). In other words, δw_j is always a small value. We hypothesize that this small perturbation due to pruning can be regarded as a noise added onto the weights and as a result a network trained with our robust strategy is more robust to both noise and pruning effect. Our experiments on CIFAR-10 and ImageNet verify that robust training has a protective effect against noise where robust coding strategies are not enough.

3.2.2. ROBUST DISTILLATION

Distillation is a well-explored NN compression technique (Hinton et al., 2015). The idea is to first train a teacher network that is large enough to capture a smooth probability distribution on labels, and then train a smaller student network by distilling the output probability information from the teacher network. We utilize distillation to optimize a compressed model (student) to be robust to PCM noise using the following noisy student loss function:

$$\begin{aligned} \mathcal{L}_s(w_s) = & (1 - \lambda)\mathbb{E}_{x,y\sim p_{\text{data}}}[-\log p_{\hat{w}_s}(y|x)] \\ & + \lambda\mathbb{E}_x[D_{KL}(p_{w_t}(y|x)||p_{g(\hat{w}_s)}(y|x))] \end{aligned}$$

where $\lambda \in [0, 1]$ is a scalar, w_t and w_s are teacher and student weights, and $g(\hat{w}_s) = g(w_s + \epsilon(w_s)) = w_s + \delta w_s$ with $\epsilon(w_s)$ being the PCM noise and δw_s being the noise injected onto the student network’s weights. We note the similarity between the noisy student loss function and loss function of the robust training. Although (Zhou et al., 2020) provides an initial exploration into robust distillation for noisy analog storage, they specifically model the noise process with white Gaussian noise, whereas we leverage experimental data collected from real storage devices to build a realistic model of the PCM noise.

3.3. End-to-End Learning

Finally, we explore an end-to-end learning approach for $g(\cdot)$ that jointly optimizes over the model compression and the known characteristics of the noisy storage device. We take a probabilistic approach and assume access to a set of weights $\{W_j\}_{j=1}^K$ from K different models that have been trained on the same dataset \mathcal{D} – this serves as an empirical distribution over NN weights, as different initializations of NNs typically converge to different local minima. Additionally, we assume that each element in the weight matrix $W_{ij} \sim \mathcal{N}(0, 1)$ (Zhou et al., 2018; Dziugaite et al., 2018).

To first learn the compressed representation of the NN weight, we propose to maximize the mutual information (MI) between the original network weight W and the compressed representation of the weight Z that has been corrupted by the noisy channel. Following (Choi et al., 2019), our coding scheme can be represented by the following Markov

chain: $W \rightarrow \hat{Z} \rightarrow Z \rightarrow \hat{W}$, where \hat{Z} denotes the compressed weight and $Z = \hat{Z} + \epsilon(Z)$ where $\epsilon(Z)$ denotes the input dependent PCM noise. Then:

$$\begin{aligned} I(W; Z) &= H(W) - H(W|Z) \\ &= -H(W|Z) \\ &\geq \mathbb{E}_{q_\phi(Z|W)}[\log p_\theta(W|Z)] \end{aligned}$$

where $q_\phi(Z|W)$ and $p_\theta(W|Z)$ denote variational approximations to the true posterior distributions $p(Z|W)$ and $p(W|Z)$, respectively (Barber & Agakov, 2003). We train an autoencoder $g_{\phi,\theta}(\cdot)$ with a stochastic encoder and decoder parameterized by ϕ, θ to learn this variational posterior via the above lower bound to the true MI. The decoder is trained to output a set of reconstructed weights such that its predictions are close to those of the original network.

For the Gaussian channel noise model, $q_\phi(Z|W)$ will be distributed according to a Gaussian distribution and the lower bound will also simplify to a difference of quadratics.

Therefore, our final objective function becomes:

$$\min_{\phi,\theta} \mathbb{E}_{x,w} [D_{KL}(p_w(y|x)||p_{g_{\phi,\theta}(\hat{w})}(y|x)) + (g_{\phi,\theta}(\hat{w}) - w)^2] \quad (2)$$

Our approach differs from KD in that we *learn* the weight compression scheme rather than using a fixed student network architecture.

4. Experimental Results

In this section, we empirically investigate: (1) whether the aforementioned protection strategies for $g(\cdot)$ help to preserve NN classification accuracy; and (2) the improvements in storage efficiency when using our protection strategies. All experimental results are averaged over 3-5 runs; for conciseness, we report only the average numbers and refer the reader to Appendix E for the complete results with confidence intervals. Hardware setup is found in Appendix A.

For all our experiments, we consider three image datasets: MNIST (LeCun et al., 2010), CIFAR-10 (Krizhevsky et al., 2009) and ImageNet (Deng et al., 2009). We use the standard train/val/test splits. For the MNIST experiments, we use two architectures: LeNet (LeCun et al., 1998), and a 3-layer MLP. For CIFAR-10, we use two types of ResNets (He et al., 2016): ResNet-18 and a slim version of ResNet-20. For ImageNet, we use pretrained ResNet-50 from PyTorch (He et al., 2016). For additional details on model architectures and hyperparameters, we refer the reader to Appendix D.

4.1. Sparsity and Sensitivity Driven Protection

We show the effect of sparsity- and sensitivity-driven protection in Figure 3 on ResNet-50 for ImageNet (Figure 6 for CIFAR-10 in Appendix). The exact numerical results

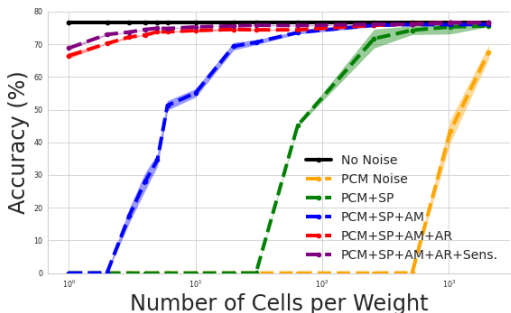


Figure 3. Accuracy of ResNet-50 on ImageNet. SP: sign protection, AM: adaptive mapping, AR: sparsity-driven adaptive redundancy, Sens.: sensitivity-driven adaptive redundancy. Experiments are conducted three times.

are given in Table 1. In CIFAR-10 experiments, the number of small weights was $N_{small} = 11\text{M}$ and the number of large weights was $N_{large} = 5.6\text{K}$ and number of cells per weight in average for adaptive redundancy is not more than 0.02 above the listed numbers in the table. Similarly, in ImageNet experiments, $N_{small} = 25.4\text{M}$, $N_{large} = 15\text{K}$ and the difference between the number of cells per weight on average and the listed number is always smaller than 0.06. These margins increase by only 0.01 when we dedicate more cells to store sensitive and large weights. As shown in Table 1, sparsity driven protection strategies are enough for ResNet-18 on CIFAR-10 to preserve the classification accuracy (95.10%) with 3 cells per weight and the accuracy is only 0.66% less than the classification accuracy with 1 cell per weight. However, there is a 4% drop in the classification accuracy of ResNet-50 on ImageNet with the number of cells per weight smaller than 4 when sparsity-driven protection is applied alone. Sensitivity driven protection is able to reduce this gap by 3%. We report the test accuracy when adaptive mapping and adaptive redundancy is applied without sign protection in (AM+AR) rows of Table 1 to show that sign protection is indeed a critical step. For instance, by comparing (AM+AR) and (SP+AM+AR) rows of Table 1, sign protection can increase the accuracy from 58% (AM+AR) to 94.4% (SP+AM+AR) on CIFAR-10.

We also consider quantization as a way to improve the efficiency of digital storage. For instance, (Jacob et al., 2018) shows that it is possible to preserve the accuracy with small loss by quantizing the weights into 8 bits. This corresponds to 4 PCM cells per weight since PCM has a capacity of 2 bits. Table 1 shows that we outperform the digital storage even when weights are quantized to 8 bits since the accuracy is preserved with 1 cell per weight on CIFAR-10 (with 0.1% loss) and with 3 cells per weight on ImageNet (with 3.6% loss). We do not compare our results with more aggressive quantization techniques (Khoram & Li, 2018; Banner et al., 2018; Oktay et al., 2019; Wiedemann et al., 2020;

Choi et al., 2020; Fan et al., 2020) that can achieve higher efficiency in digital storage since they also bring a huge complexity with multiple retraining stages.

We also combine the sparsity driven protection with pruning to gain further storage efficiency improvements. Results on sparsity driven protection strategies on 90% pruned ResNet-18 (on CIFAR-10) are in Appendix E.2. We retrain the pruned model for 20 epochs to tune the nonzero weights. The accuracy of the pruned model without noise is 94.8% and we get 94.2% test accuracy with PCM noise using only 1 cell per weight. Compared to the baseline (no compression and each 32-bit weight is digitally stored on 16 PCM cells), we provide $16 \times 10 = 160$ times more efficient storage with 90% pruning and using 1 cell per weight.

4.2. Robust Training

We compare robust training with naive training (training with no noise) in Table 2 on ResNet-18 (on CIFAR-10) and on ResNet-50 (on ImageNet). In our experiments, we use $\lambda = 0.5$ as the coefficient of the KL divergence term in the loss function. We tried different combinations of the sparsity and sensitivity driven strategies, and in all cases, robust training provides better robustness against PCM noise than the naive training. Robust training provides robustness against pruning as well. When ResNet-18 trained without noise is pruned with 90% sparsity, the accuracy drops from 95.1% to 90.2%. However, the same model trained with $N(0, 0.006)$ gives 95.0% accuracy after 90% pruning.

	Naive Train (no noise)	Robust Train (with $N(0, 0.01)$)	Robust Train (with $N(0, 0.006)$)	Add. Bits	
CIFAR-10	No Noise	95.10	95.50	95.60	0
	PCM (No Protection)	9.70	8.30	9.90	0
	PCM+SP	9.70	10.63	10.33	1
	PCM+AP	27.69	86.20	81.83	1
	PCM+SP+AP	90.60	94.73	94.80	2
	PCM+AP+Sens	36.21	86.73	78.93	2
	PCM+SP+AP+Sens	94.95	95.03	95.03	3
ImageNet	No Noise	76.60	76.60	76.60	0
	PCM (No Protection)	0.001	0.001	0.001	0
	PCM+SP	0.001	0.004	0.002	1
	PCM+AP	0.001	0.002	0.001	1
	PCM+SP+AP	66.00	69.00	69.20	2
	PCM+AP+Sens	0.003	0.006	0.005	2
	PCM+SP+AP+Sens	68.80	70.20	70.40	3

Table 2. Robust training vs. naive training for ResNet-18 on CIFAR-10 and ResNet-50 on ImageNet. SP: sign protection, AP: adaptive protection (adaptive mapping+sparsity-driven adaptive redundancy), Sens.: sensitivity-driven adaptive redundancy.

4.3. Robust Distillation

Table 3 shows the distillation results on ResNet-20 distilled from ResNet-18 (on CIFAR-10) with PCM noise applied during test time. We compare three networks: (1) a student ResNet-20 distilled without noise injection, (2) a student ResNet-20 distilled with Gaussian noise injection, and (3)

	Number of PCM cells	Teacher ResNet-18	Teacher ResNet-20	Student ResNet-20	Noisy Student ResNet-20	Add. Bits
No Noise	16	95.70	92.50	92.90	93.00	0
PCM+AP	3	16.23	48.38	73.38	81.75	1
PCM+SP+AP	1	93.35	86.30	88.58	90.65	2
	3	94.78	89.73	89.98	91.33	
PCM+AP+Sens.	1	9.60	29.68	38.18	69.49	2
PCM+SP+AP+Sens.	1	93.36	88.40	88.96	91.10	3
	3	94.90	89.92	90.44	91.78	

Table 3. Accuracy of ResNet-20 distilled from ResNet-18 on CIFAR-10. SP: sign protection, AP: adaptive protection (adaptive mapping+sparsity-driven adaptive redundancy), Sens.: sensitivity-driven adaptive redundancy. During the distillation of noisy student, a Gaussian noise with $N(0,0.01)$ is injected onto the weights.

a teacher ResNet-20 (a baseline) trained without noise. As shown in Table 3, student ResNet-20 distilled with noise injection outperforms both teacher ResNet-20 and student ResNet-20 distilled without noise when weights are perturbed by PCM cells at test time. For additional results with Gaussian noise injected at test time and additional experiments on MNIST, we refer the reader to Appendix E.4.

4.4. End-to-End Learning

Next, we explore the effectiveness of the end-to-end learning scheme in which we train an autoencoder on a *set of model weights* on a synthetic example. We generate two sets of 2-D Gaussian mixtures: (1) an “easy” task in which we first sample a two-dimensional mean vector $\mu_1 \in \mathbb{R}^2$ where $\mu_{1i} \sim \mathcal{U}[-1, 0)$ and $\mu_2 \in \mathbb{R}^2$ where $\mu_{2i} \sim \mathcal{U}[0, 1)$ for $i = \{1, 2\}$. After sampling these means, we draw a set of 50K points for the two mixture components: $x_1 \sim \mathcal{N}(\mu_1, I)$ and $x_2 \sim \mathcal{N}(\mu_2, I)$. This ensures that the two mixture components are well-separated. For the “hard” task, we sample overlapping mean vectors: both components of μ_1 and μ_2 are drawn from $\mathcal{U}[-1, +1]$ before sampling from their respective Gaussian mixture components. We generate 50 datasets per task, where each dataset has 50K data points.

We train 50 different logistic regression models on each of the datasets for both the “easy” and “hard” tasks (each model has 3 parameters). Then, we train an autoencoder on these sets of weights for both Gaussian and PCM channel noise. For the easy task with Gaussian noise, the autoencoder achieves an accuracy of 95.2%; for PCM noise, it achieves 91.8% accuracy. For the hard task with Gaussian noise, the autoencoder achieves an average accuracy of 78.8% across all classifiers; for PCM channel noise, it achieves 78.6% on average across all 50 classifiers. Interestingly, we find that the 1-D classifier representations in the autoencoder’s latent space is semantically meaningful (Appendix E.5).

5. Related Work

Model Compression. Compression of NN parameters has a rich history starting from the early works of (Cun et al., 1990; Hassibi et al., 1993), with techniques such as pruning (Han et al., 2015; 2016; Lee et al., 2018; Frankle & Carbin, 2019; Singh & Alistarh, 2020; Sehwag et al., 2020), quantization (Khoram & Li, 2018; Banner et al., 2018; Choi et al., 2020; Fan et al., 2020) and KD (Hinton et al., 2015; Polino et al., 2018; Xie et al., 2020). (Papernot et al., 2016) explores KD as a way to encourage robustness to adversarial perturbations in input space, while we specifically desire robustness to weight perturbations. Although probabilistic approaches to model compression have been explored in (Louizos et al., 2017; Reagan et al., 2018; Havasi et al., 2019), we additionally consider the physical constraints of the storage device used for memory as part of our learning scheme. Our end-to-end approach is most similar to (Oktay et al., 2019), in that they also learn a decoder to map NN weights into a latent space prior to quantization. However, our method is different in that our autoencoder also learns the appropriate compression scheme (with an encoder), we inject noise into our compressed weights rather than quantizing, and we do not require training a NN from scratch.

Analog Computing in NNs. A complementary line of work exists on utilizing analog components in NN training and/or inference (Schmid et al., 2000; Bo et al., 2000; Binas et al., 2016; Du et al., 2018; Burr et al., 2019; Joshi et al., 2020). The common theme is performing computation in the analog domain, perhaps with in-memory computation capabilities, in order to reduce the overall computation power. However, analog computing comes with its own complexities such as inherent noise or lack of flexibility. In contrast, our work only focuses on storing NN models in analog cells and our objective is to increase storage density. Once the parameters are read from memory, the actual computation happens in the conventional digital domain.

6. Conclusion

In this work, we formalized the problem of jointly learning the model compression and physical storage to maximize memory utility in noisy analog storage devices. We introduced a variety of novel coding techniques for preserving NN classification accuracy even in the presence of weight perturbations, and demonstrated their effectiveness on MNIST, CIFAR-10, and ImageNet. Additionally, we explored different training strategies that can be coupled with existing compression techniques such as distillation, and provided an initial foray into a fully end-to-end learning scheme for the joint problem. Extending our framework to allow for quantization would be interesting future work, as well as exploring how to handle models trained on a variety of datasets and tasks in the end-to-end learning scheme.

7. Acknowledgement

The authors would like to thank TSMC Corporate Research for technical discussions. This work was supported in part by a Sony Stanford Graduate Fellowship.

References

- Achille, A., Paolini, G., and Soatto, S. Where is the information in a deep neural network? *arXiv preprint arXiv:1905.12213*, 2019.
- Banner, R., Hubara, I., Hoffer, E., and Soudry, D. Scalable methods for 8-bit training of neural networks. In *Advances in neural information processing systems*, pp. 5145–5153, 2018.
- Barber, D. and Agakov, F. V. The im algorithm: a variational approach to information maximization. In *Advances in neural information processing systems*, pp. None, 2003.
- Binas, J., Neil, D., Indiveri, G., Liu, S.-C., and Pfeiffer, M. Precise neural network computation with imprecise analog devices. *arXiv preprint arXiv:1606.07786*, 2016.
- Bo, G. M., Caviglia, D. D., and Valle, M. An on-chip learning neural network. In *Proceedings of the IEEE-INNS-ENNS International Joint Conference on Neural Networks. IJCNN 2000. Neural Computing: New Challenges and Perspectives for the New Millennium*, volume 4, pp. 66–71 vol.4, 2000. doi: 10.1109/IJCNN.2000.860751.
- Bucilua, C., Caruana, R., and Niculescu-Mizil, A. Model compression. In *Proceedings of the 12th ACM SIGKDD International Conference on Knowledge Discovery and Data Mining, KDD '06*, pp. 535–541, New York, NY, USA, 2006. Association for Computing Machinery. ISBN 1595933395. doi: 10.1145/1150402.1150464. URL <https://doi.org/10.1145/1150402.1150464>.
- Burr, G. W., Ambrogio, S., Narayanan, P., Tsai, H., Mackin, C., and Chen, A. Accelerating deep neural networks with analog memory devices. In *2019 China Semiconductor Technology International Conference (CSTIC)*, pp. 1–3, 2019. doi: 10.1109/CSTIC.2019.8755642.
- Cheng, Y., Wang, D., Zhou, P., and Zhang, T. Model compression and acceleration for deep neural networks: The principles, progress, and challenges. *IEEE Signal Processing Magazine*, 35(1):126–136, 2018.
- Choi, K., Tatwawadi, K., Grover, A., Weissman, T., and Ermon, S. Neural joint source-channel coding. In *International Conference on Machine Learning*, pp. 1182–1192. PMLR, 2019.
- Choi, Y., El-Khamy, M., and Lee, J. Universal deep neural network compression. *IEEE Journal of Selected Topics in Signal Processing*, 2020.
- Cun, Y. L., Denker, J. S., and Solla, S. A. *Optimal Brain Damage*, pp. 598–605. Morgan Kaufmann Publishers Inc., San Francisco, CA, USA, 1990. ISBN 1558601007.
- Dean, J., Corrado, G., Monga, R., Chen, K., Devin, M., Mao, M., Ranzato, M., Senior, A., Tucker, P., Yang, K., et al. Large scale distributed deep networks. In *Advances in neural information processing systems*, pp. 1223–1231, 2012.
- Deng, J., Dong, W., Socher, R., Li, L.-J., Li, K., and Fei-Fei, L. ImageNet: A Large-Scale Hierarchical Image Database. In *CVPR09*, 2009.
- Du, Y., Du, L., Gu, X., Du, J., Wang, X. S., Hu, B., Jiang, M., Chen, X., Iyer, S. S., and Chang, M.-C. F. An analog neural network computing engine using cmos-compatible charge-trap-transistor (ctt). *IEEE Transactions on Computer-Aided Design of Integrated Circuits and Systems*, 38(10):1811–1819, 2018.
- Dziugaite, G. K., Arpino, G., and Roy, D. M. Towards generalization guarantees for sgd: Data-dependent pac-bayes priors. 2018.
- Fagbohunge, O. and Qian, L. Benchmarking inference performance of deep learning models on analog devices. *arXiv preprint arXiv:2011.11840*, 2020.
- Fan, A., Stock, P., Graham, B., Grave, E., Gribonval, R., Jégou, H., and Joulin, A. Training with quantization noise for extreme model compression. 2020.
- Frankle, J. and Carbin, M. The lottery ticket hypothesis: Finding sparse, trainable neural networks. *International Conference on Learning Representations (ICLR)*, 2019.
- Grosse, R. and Martens, J. A kronecker-factored approximate fisher matrix for convolution layers. In *International Conference on Machine Learning*, pp. 573–582, 2016.
- Guo, Y., Yao, A., and Chen, Y. Dynamic network surgery for efficient dnns. In *Advances in neural information processing systems*, pp. 1379–1387, 2016.
- Han, S., Pool, J., Tran, J., and Dally, W. Learning both weights and connections for efficient neural network. In *Advances in neural information processing systems*, pp. 1135–1143, 2015.
- Han, S., Mao, H., and Dally, W. J. Deep compression: Compressing deep neural networks with pruning, trained quantization and huffman coding. *International Conference on Learning Representations (ICLR)*, 2016.

- Hassibi, B., Stork, D. G., Wolff, G., and Watanabe, T. Optimal brain surgeon: Extensions and performance comparisons. In *Proceedings of the 6th International Conference on Neural Information Processing Systems, NIPS'93*, pp. 263–270, San Francisco, CA, USA, 1993.
- Havasi, M., Peharz, R., and Hernández-Lobato, J. M. Minimal random code learning: Getting bits back from compressed model parameters. In *International Conference on Learning Representations (ICLR)*, 2019.
- He, K., Zhang, X., Ren, S., and Sun, J. Deep residual learning for image recognition. In *Proceedings of the IEEE conference on computer vision and pattern recognition*, pp. 770–778, 2016.
- Hinton, G., Vinyals, O., and Dean, J. Distilling the knowledge in a neural network. In *NIPS Deep Learning and Representation Learning Workshop*, 2015. URL <http://arxiv.org/abs/1503.02531>.
- Jacob, B., Kligys, S., Chen, B., Zhu, M., Tang, M., Howard, A., Adam, H., and Kalenichenko, D. Quantization and training of neural networks for efficient integer-arithmetic-only inference. In *Proceedings of the IEEE Conference on Computer Vision and Pattern Recognition*, pp. 2704–2713, 2018.
- Joshi, V., Gallo, M. L., Haefeli, S., Boybat, I., Nandakumar, S., Piveteau, C., Dazzi, M., Rajendran, B., Sebastian, A., and Eleftheriou, E. Accurate deep neural network inference using computational phase-change memory. *Nature Communications*, 11, 2020.
- Khoram, S. and Li, J. Adaptive quantization of neural networks. In *International Conference on Learning Representations*, 2018.
- Krizhevsky, A., Hinton, G., et al. Learning multiple layers of features from tiny images. 2009.
- LeCun, Y., Bottou, L., Bengio, Y., and Haffner, P. Gradient-based learning applied to document recognition. *Proceedings of the IEEE*, 86(11):2278–2324, 1998.
- LeCun, Y., Cortes, C., and Burges, C. Mnist handwritten digit database, 2010.
- LeCun, Y., Bengio, Y., and Hinton, G. Deep learning. *nature*, 521(7553):436–444, 2015.
- Lee, N., Ajanthan, T., and Torr, P. H. Snip: Single-shot network pruning based on connection sensitivity. *arXiv preprint arXiv:1810.02340*, 2018.
- Louizos, C., Ullrich, K., and Welling, M. Bayesian compression for deep learning. *arXiv preprint arXiv:1705.08665*, 2017.
- Martens, J. New insights and perspectives on the natural gradient method. *arXiv preprint arXiv:1412.1193*, 2014.
- Oktay, D., Ballé, J., Singh, S., and Shrivastava, A. Scalable model compression by entropy penalized reparameterization. *arXiv preprint arXiv:1906.06624*, 2019.
- Papernot, N., McDaniel, P., Wu, X., Jha, S., and Swami, A. Distillation as a defense to adversarial perturbations against deep neural networks. In *2016 IEEE Symposium on Security and Privacy (SP)*, pp. 582–597. IEEE, 2016.
- Polino, A., Pascanu, R., and Alistarh, D. Model compression via distillation and quantization. *arXiv preprint arXiv:1802.05668*, 2018.
- Reagan, B., Gupta, U., Adolf, B., Mitzenmacher, M., Rush, A., Wei, G.-Y., and Brooks, D. Weightless: Lossy weight encoding for deep neural network compression. In *International Conference on Machine Learning*, pp. 4324–4333, 2018.
- Schmid, A., Leblebici, Y., and Mlynek, D. Mixed analogue-digital artificial-neural-network architecture with on-chip learning. *Circuits, Devices and Systems, IEE Proceedings* -, 146:345 – 349, 01 2000. doi: 10.1049/ip-cds:19990685.
- Sehwag, V., Wang, S., Mittal, P., and Jana, S. Hydra: Pruning adversarially robust neural networks. *Advances in Neural Information Processing Systems (NeurIPS)*, 7, 2020.
- Shannon, C. E. A mathematical theory of communication. *ACM SIGMOBILE mobile computing and communications review*, 5(1):3–55, 2001.
- Singh, S. P. and Alistarh, D. Woodfisher: Efficient second-order approximations for model compression. *arXiv preprint arXiv:2004.14340*, 2020.
- Upadhyaya, P., Yu, X., Mink, J., Cordero, J., Parmar, P., and Jiang, A. A. Error correction for hardware-implemented deep neural networks. 2019.
- Wiedemann, S., Kirchhoffer, H., Matlage, S., Haase, P., Marban, A., Marinč, T., Neumann, D., Nguyen, T., Schwarz, H., Wiegand, T., Marpe, D., and Samek, W. Deepcabac: A universal compression algorithm for deep neural networks. *IEEE Journal of Selected Topics in Signal Processing*, 14(4):700–714, 2020.
- Wong, H.-S. P., Raoux, S., Kim, S., Liang, J., Reifenberg, J. P., Rajendran, B., Asheghi, M., and Goodson, K. E. Phase change memory. *Proceedings of the IEEE*, 98(12): 2201–2227, 2010.
- Xie, Q., Luong, M.-T., Hovy, E., and Le, Q. V. Self-training with noisy student improves imagenet classification. In

Proceedings of the IEEE/CVF Conference on Computer Vision and Pattern Recognition, pp. 10687–10698, 2020.

Zarcone, R., Paiton, D., Anderson, A., Engel, J., Wong, H. P., and Olshausen, B. Joint source-channel coding with neural networks for analog data compression and storage. In *2018 Data Compression Conference*, pp. 147–156. IEEE, 2018.

Zarcone, R. V., Engel, J. H., Eryilmaz, S. B., Wan, W., Kim, S., BrightSky, M., Lam, C., Lung, H.-L., Olshausen, B. A., and Wong, H.-S. P. Author correction: Analog coding in emerging memory systems. *Scientific reports*, 10(1):13404, August 2020. ISSN 2045-2322. doi: 10.1038/s41598-020-70121-y. URL <https://europepmc.org/articles/PMC7400509>.

Zheng, X., Zarcone, R., Paiton, D., Sohn, J., Wan, W., Olshausen, B., and Wong, H.-S. P. Error-resilient analog image storage and compression with analog-valued rram arrays: an adaptive joint source-channel coding approach. In *2018 IEEE International Electron Devices Meeting (IEDM)*, pp. 3–5. IEEE, 2018.

Zhou, C., Kadambi, P., Mattina, M., and Whatmough, P. N. Noisy machines: Understanding noisy neural networks and enhancing robustness to analog hardware errors using distillation. *arXiv preprint arXiv:2001.04974*, 2020.

Zhou, W., Veitch, V., Austern, M., Adams, R. P., and Orbanz, P. Non-vacuous generalization bounds at the imagenet scale: a pac-bayesian compression approach. *arXiv preprint arXiv:1804.05862*, 2018.

Appendix

A. Additional Details on PCM Arrays

The measurement data used in the paper to model the PCM channel noise is collected on a PCM array with one mega cells. The memory cells are first at initial state and then programmed with electrical pulses. The physical state of the memory cell (output) would be continuously tuned with different programming pulse amplitude (input). To collect the measurement data for this work, we programmed the array with 31 different pulse amplitudes and more than 1000 cells for each pulse amplitude. Figure 4(a) shows the 1-standard deviation error bar from cell-to-cell variation for each input level, where both the mean and standard deviation of the output is non-linearly related to the input. Figure 4(b) is the histogram of output distributions corresponding to 31 input levels, which shows that the output is roughly Gaussian distributed conditioned on the input level. The channel response to the input values in between measurement points is then interpolated in order to construct the differentiable continuous analog channel model used in this work as shown in Figure 4(c). The differentiability of the model allows for an end-to-end learning scheme as shown in Figure 7.

B. Multiple Channel Usages

In this section, we provide additional details on the noisy channel and investigate how the noise changes as we play with the scale factor α and the number of channel usages r . Suppose we have a zero-mean noisy storage channel ϕ with a power constraint $|w_{in}| \leq P$, where w_{in} is the input weights that is to be stored on the channel and P is the power constraint ($P = 1$ in our experiments). We must first map all the inputs w_{in} such that they will fit within the range $[-P, P]$ to respect the physical constraints of the PCM storage device. Then, the relationship between the input weights w_{in} to be stored and the output weights w_{out} to be read is:

$$w_{out} = \frac{\phi(\alpha \cdot w_{in} - \beta) + \beta}{\alpha}$$

where α and β are scale and shift factors, respectively. Since the noise is zero-mean, we have:

$$w_{out} = \frac{\alpha \cdot w_{in} - \beta + \epsilon_0(w_{in}) + \beta}{\alpha} = w_{in} + \frac{\epsilon_0(w_{in})}{\alpha}$$

where $\epsilon_0(w_{in})$ is zero-mean noise with input dependent standard deviation $\sigma(w_{in})$. If we use the noisy channel ϕ r times to store the same weight (r cells per weight), we can average over the outputs:

$$\begin{aligned} w_{out} &= \frac{1}{r} \sum_{i=1}^r \left(w_{in} + \frac{\epsilon_{0,i}(w_{in})}{\alpha} \right) \\ &= w_{in} + \frac{1}{r} \sum_{i=1}^r \frac{\epsilon_{0,i}(w_{in})}{\alpha} \end{aligned} \quad (3)$$

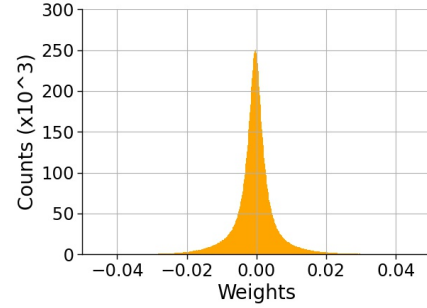
Let us define a new random variable $\tilde{\epsilon}(w_{in}, r) = \frac{1}{r} \sum_{i=1}^r \epsilon_{0,i}(w_{in})$. Notice that the standard deviation of $\tilde{\epsilon}(w_{in}, r)$ is $\frac{\sigma(w_{in})}{\sqrt{r}}$. Then the standard deviation of $\hat{\epsilon}(w_{in}, r, \alpha) = \frac{\tilde{\epsilon}(w_{in}, r)}{\alpha}$ in Eq. 3 is given by: $\frac{\sigma(w_{in})}{\alpha\sqrt{r}}$. More precisely, we have the following expression:

$$w_{out} = w_{in} + \hat{\epsilon}(w_{in}, r, \alpha)$$

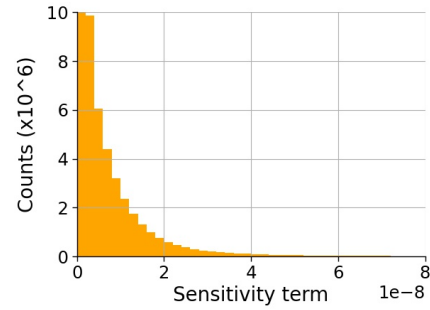
where the standard deviation of $\hat{\epsilon}(w_{in}, r, \alpha)$ is $\frac{\sigma(w_{in})}{\alpha\sqrt{r}}$.

C. Sparsity of Neural Network Weights and Gradients

Figure 5 shows the histogram of weights and sensitivity terms ($s_j = \frac{1}{N} \sum_{i=1}^N \left(\frac{\partial \log p_w(y_i|x_i)}{\partial w_j} \right)^2$ from Section 3.1.2) of ResNet-18 after it is trained on CIFAR-10. The sparsity of the weights and sensitivity terms are critical in our experiments since we use more PCM cells for weights with larger magnitudes and larger sensitivities, assuming that this adaptive strategy has a negligible effect on the average number of cells per weight.



(a) Distribution of weights (ResNet-18 trained on CIFAR-10).



(b) Distribution of sensitivity terms (ResNet-18 trained on CIFAR-10).

Figure 5. Histogram of (a) weights of ResNet-18 trained on CIFAR-10, (b) sensitivity terms of ResNet-18 trained on CIFAR-10. Since both the weights and sensitivities are sparse, the increase in the average number of cells per weight due to adaptive redundancy and sensitivity-driven protection strategies is negligible.

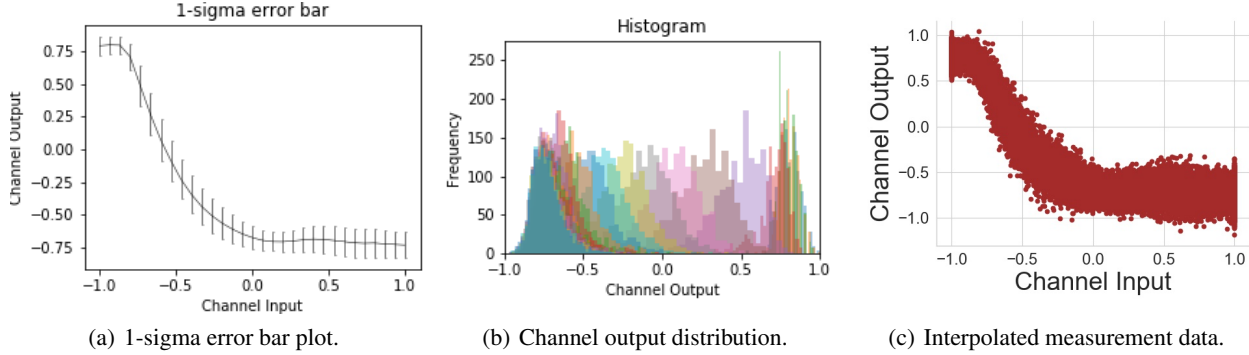


Figure 4. Characteristics of the channel noise in a PCM cell. (a) 1-standard deviation error bars for each input level, where both the mean and variation of the output has a nonlinear relationship to the input value. (b) Distribution of output values corresponding to 31 distinct input values into the PCM array. (c) Channel response values for the PCM array.

D. Additional Experimental Details

In the following subsection, we provide additional details on the models, model architectures, and hyperparameters used in our experiments.

D.1. MNIST

We provide the architectural details and hyperparameters for LeNet and the MLP in Tables 4 and 5 respectively:

Name	Component
conv1	5×5 conv, 20 filters, stride 1], ReLU, 2×2 max pool
conv2	5×5 conv, 50 filters, stride 1], ReLU, 2×2 max pool
Linear	Linear $800 \rightarrow 500$, ReLU
Output Layer	Linear $500 \rightarrow 10$

Table 4. LeNet architecture for MNIST experiments.

Name	Component
Input Layer	Linear $784 \rightarrow 100$, ReLU
Hidden Layer	Linear $100 \rightarrow 100$, ReLU
Output Layer	Linear $100 \rightarrow 10$

Table 5. MLP architecture for MNIST experiments.

For both the LeNet and MLP classifiers, we use a batch size of 100 and train for 100 epochs, early stopping at the best accuracy on the validation set. We use the Adam optimizer with learning rate = 0.001, and $\beta_1 = 0.9, \beta_2 = 0.999$ with weight decay = $5e^{-4}$. For knowledge distillation, we use a temperature parameter of $T = 1.5$ and equally weight the contributions of the student network’s cross entropy loss and the distillation loss ($\lambda = 0.5$).

D.2. CIFAR-10

We provide the architectural details and hyperparameters for the ResNet-18 and the slim ResNet-20 used in our experiments in Tables 6 and 7 below:

Name	Component
conv1	3×3 conv, 64 filters, stride 1, BatchNorm
Residual Block 1	3×3 conv, 64 filters 3×3 conv, 64 filters $\times 2$
Residual Block 2	3×3 conv, 128 filters 3×3 conv, 128 filters $\times 2$
Residual Block 3	3×3 conv, 256 filters 3×3 conv, 256 filters $\times 2$
Residual Block 4	3×3 conv, 512 filters 3×3 conv, 512 filters $\times 2$
Output Layer	4×4 average pool stride 1, fully-connected, softmax

Table 6. ResNet-18 architecture for CIFAR-10 experiments.

Name	Component
conv1	3×3 conv, 16 filters, stride 1, BatchNorm
Residual Block 1	3×3 conv, 16 filters 3×3 conv, 16 filters $\times 2$
Residual Block 2	3×3 conv, 32 filters 3×3 conv, 32 filters $\times 2$
Residual Block 3	3×3 conv, 64 filters 3×3 conv, 64 filters $\times 2$
Output Layer	7×7 average pool stride 1, fully-connected, softmax

Table 7. Slim ResNet-20 architecture for CIFAR-10 experiments.

For both ResNet-18 and slim ResNet-20, we use a batch size of 128 and train for 350 epochs, early stopping at the best accuracy on the validation set. We use SGD with learning rate = 0.1, and momentum = 0.9 and weight decay = $5e^{-4}$.

D.3. IMAGENET

We provide the architectural details and hyperparameters for the ResNet-50 used in our experiments in Table 8.

We use the pretrained ResNet-50 from PyTorch (<https://github.com/pytorch/vision/blob/master/torchvision/models/resnet.py>), with a batch size of 64. For the robust training experiments, we retrain the model for 20 epochs with early stopping at

Name	Component	
conv1	3 × 3 conv, 64 filters, stride 1, BatchNorm	
Residual Block 1	1 × 1 conv, 64 filters 3 × 3 conv, 64 filters 1 × 1 conv, 256 filters	× 3
Residual Block 2	1 × 1 conv, 128 filters 3 × 3 conv, 128 filters 1 × 1 conv, 512 filters	× 4
Residual Block 3	1 × 1 conv, 256 filters 3 × 3 conv, 256 filters 1 × 1 conv, 1024 filters	× 6
Residual Block 4	1 × 1 conv, 512 filters 3 × 3 conv, 512 filters 1 × 1 conv, 2048 filters	× 3
Output Layer	4 × 4 average pool stride 1, fully-connected, softmax	

Table 8. ResNet-50 architecture for ImageNet experiments.

best accuracy. We use SGD with learning rate = 0.001, and momentum = 0.9 and weight decay = $5e^{-4}$.

E. Additional Experimental Results

E.1. SPARSITY- AND SENSITIVITY-DRIVEN PROTECTION

We give the full results of sparsity-driven and sensitivity-driven protection experiments on CIFAR-10 and ImageNet with confidence intervals in Table 9 and Table 10. In Figure 6, we present experimental results with ResNet-18 on CIFAR-10. As can be seen from Figure 6(a), our strategies, namely sign protection, adaptive mapping and adaptive redundancy, reduce the number of PCM cells per weight required to preserve accuracy from 1024 to 1. We also test our strategies against Gaussian noise. In the Gaussian experiments, we consider hypothetical storage devices with white Gaussian noise where the standard deviation of the overall noise on the output ($\hat{\epsilon}(r, \alpha)$ “not input-dependent”) can be reduced by using the channel multiple times (Method #1) and by using the channel in the its power limit (Method #2). Figure 6(b) shows that our strategies increase the standard deviation threshold, where the NN performance sharply drops, from 0.005 to 0.2, i.e., robustness increases by 40 times. We note that we present results of Gaussian noise experiments to be comparable to future work although this scenario is not realistic.

E.2. ROBUST PRUNING

We give the full results of robust pruning experiment with confidence intervals in Table 11. We apply one-shot pruning followed by 20 epochs of retraining. When sparsity- and sensitivity-driven strategies are applied, 3 cells per weight are enough to preserve the original accuracy of the pruned model (94.8%). Moreover, if we use only 1 cell per weight on average, the accuracy drop is 0.1%, which is insignificant considering the fact that pruning reduces the accuracy by 0.3% (from 95.1% to 94.8%). We note that this perform-

ance degradation due to pruning can be eliminated with robust training, explained in Section 3.2.1. Without pruning, the sparsity- and sensitivity- driven protection strategies provide 16 times improvement in the memory efficiency since the number of cells per weight required to preserve the accuracy drops from 16 to 1 when we use analog storage instead of digital storage. As our strategies work well with pruning from Table 11, we get further memory efficiency, e.g., $10 \times 16 = 160$ times more efficient storage with 90% pruning.

E.3. ROBUST TRAINING

We give the full results of robust training experiments on CIFAR-10 and ImageNet with confidence intervals in Table 12 and Table 13. We use $\lambda = 0.5$ as the coefficient of the KL regularization term in the loss function in Section 3.2.1. The level of the noise (standard deviation) injected during the training is adjusted according to r and α values to be used at storage time since the noise at storage time has a standard deviation of $\frac{\sigma(w_{in})}{\alpha\sqrt{r}}$. It is seen from Table 12 and Table 13 that robust training improves the robustness of the network against noise. We have also observed that the pruned network reaches higher accuracy after robust training compared to naive training without noise injection (an increase from 90.2% to 95.0% without retraining).

E.4. ROBUST DISTILLATION

Knowledge distillation (KD) is a well-established NN compression method where a large teacher network is trained with \mathcal{L}_t loss given by

$$\mathcal{L}_t = \mathbb{E}_{x,y \sim p_{data}} [-\log p_{w_t}(y|x)]$$

where w_t is the weights of the teacher network, and probability of each class i is the output of the high temperature softmax activation applied to logits:

$$y_i = \frac{\exp(z_i/T)}{\sum_j \exp(z_j/T)}$$

where z_i is the logit for class i . Temperature $T > 1$ helps the output probabilities of the teacher network be softer. Using the same temperature, a smaller student network can be trained with the following student loss function \mathcal{L}_s :

$$\mathcal{L}_s = (1 - \lambda)\mathbb{E}_{x,y \sim p_{data}} [-\log p_{w_s}(y|x)] + \lambda\mathbb{E}_x [D_{KL}(p_{w_t}(y|x)||p_{w_s}(y|x))]$$

where w_s is the weights of the student network. It has been shown that distilled student network achieves a test accuracy that a teacher network with the same architecture cannot achieve. In other words, a student network distilled from a teacher network performs comparable to a larger network. This suggests that knowledge distillation can be

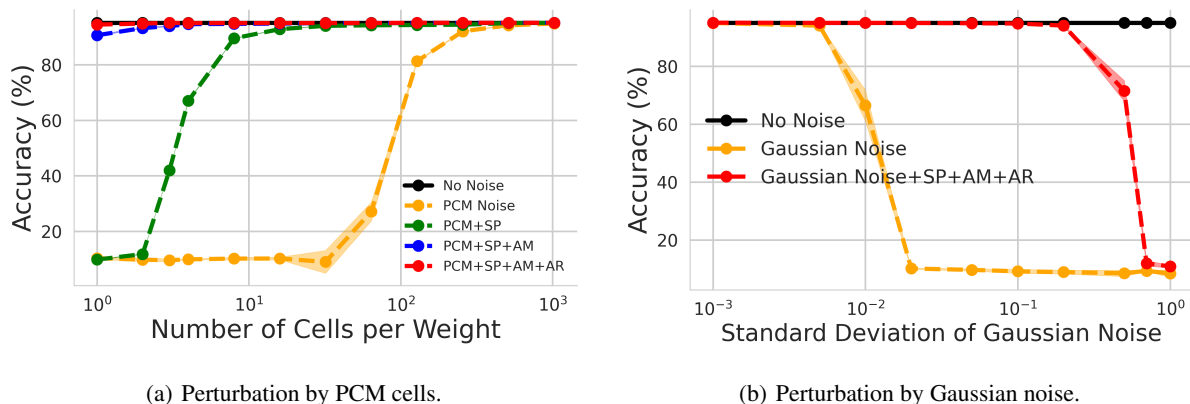


Figure 6. Accuracy of ResNet-18 on CIFAR-10 when weights are perturbed by (a) PCM cells, (b) Gaussian noise. SP: sign protection, AM: adaptive mapping, AR: sparsity-driven adaptive redundancy. Experiments are conducted three times.

	512 cells	64 cells	32 cells	16 cells	8 cells	4 cells	3 cells	2 cells	1 cell	Additional Bits
No Protection	94.2(± 0.1)	27.1 (± 3.4)	9.0 (± 4.1)	10.2 (± 0.5)	10.2 (± 0.5)	9.9 (± 0.1)	9.6 (± 0.5)	9.8 (± 0.7)	10.3 (± 0.4)	0
SP	95.0 (± 0.0)	94.2 (± 0.1)	94.00 (± 0.2)	92.80 (± 0.3)	89.50 (± 0.6)	67.00 (± 0.2)	41.90 (± 0.5)	11.80 (± 5.1)	9.80 (± 1.5)	1
AM+AR	95.0 (± 0.0)	94.8 (± 0.1)	94.70 (± 0.1)	94.40 (± 0.1)	93.70 (± 0.2)	93.10 (± 0.2)	92.70 (± 0.2)	89.20 (± 2.6)	58.00 (± 8.2)	1
SP+AM	95.1 (± 0.0)	95.0 (± 0.0)	95.00 (± 0.1)	94.80 (± 0.1)	94.70 (± 0.1)	94.60 (± 0.1)	93.90 (± 0.2)	93.20 (± 0.1)	90.60 (± 0.3)	2
SP+AM+AR	95.1 (± 0.0)	95.0 (± 0.0)	95.00 (± 0.1)	95.00 (± 0.1)	95.00 (± 0.1)	95.00 (± 0.1)	95.10 (± 0.1)	94.80 (± 0.1)	94.44 (± 0.2)	2
SP+AM+AR+Sens.	95.1 (± 0.0)	95.1 (± 0.0)	95.10 (± 0.1)	95.07 (± 0.1)	95.11 (± 0.1)	95.03 (± 0.2)	95.14 (± 0.1)	94.80 (± 0.1)	94.95 (± 0.3)	3

Table 9. Accuracy of ResNet-18 on CIFAR-10 when weights are perturbed by the PCM cells. Baseline accuracy (when there is no noise) is 95.10%. SP: sign protection, AM: adaptive mapping, AR: sparsity-driven adaptive redundancy, Sens.: sensitivity-driven adaptive redundancy. Reported results are averaged over three experimental runs.

	512 cells	64 cells	32 cells	16 cells	8 cells	4 cells	3 cells	2 cells	1 cell	Additional Bits
No Protection	0.001(± 0.0)	0.001 (± 0.0)	0.001 (± 0.0)	0.001 (± 0.0)	0.001 (± 0.0)	0.001 (± 0.0)	0.001 (± 0.0)	0.001 (± 0.0)	0.001 (± 0.0)	0
SP	0.044(± 0.0)	0.009 (± 0.0)	0.001 (± 0.0)	0.001 (± 0.0)	0.001 (± 0.0)	0.001 (± 0.0)	0.001 (± 0.0)	0.001 (± 0.0)	0.001 (± 0.0)	1
AM+AR	75.0 (± 0.5)	66.7 (± 0.8)	66.4 (± 2.5)	63.2 (± 2.5)	57.5 (± 2.2)	34.1 (± 3.4)	22.4 (± 3.0)	0.037 (± 0.0)	0.001 (± 0.0)	2
SP+AM	70.6 (± 0.7)	69.4 (± 1.1)	55.1 (± 3.2)	51.3 (± 2.4)	34.6 (± 1.8)	28.0 (± 5.6)	17.6 (± 4.1)	0.046 (± 0.0)	0.002 (± 0.0)	2
SP+AM+AR	75.4 (± 0.2)	74.5 (± 0.1)	74.2 (± 0.4)	73.8 (± 0.0)	73.8 (± 0.2)	72.8 (± 0.0)	72.2 (± 0.4)	70.2 (± 0.0)	66.0 (± 0.8)	1
SP+AM+AR+Sens.	75.8 (± 0.0)	75.6 (± 0.0)	75.3 (± 0.0)	74.8 (± 0.1)	74.9 (± 0.1)	74.5 (± 0.1)	73.7 (± 0.0)	73.0 (± 0.2)	68.8 (± 0.3)	3

Table 10. Accuracy of ResNet-50 on ImageNet when weights are perturbed by the PCM cells. Baseline accuracy (when there is no noise) is 76.6%. SP: sign protection, AM: adaptive mapping, AR: sparsity-driven adaptive redundancy, Sens.: sensitivity-driven adaptive redundancy. Reported results are averaged over three experimental runs.

	10 cells	5 cells	3 cells	2 cells	1 cell	Additional Bits
No Protection	10.1 (± 0.2)	9.2 (± 0.3)	9.9 (± 0.3)	(± 0.1) 10.1 (± 0.4)	9.1 (± 0.3)	0
SP	76.5 (± 0.1)	22.5 (± 1.1)	13.1 (± 0.8)	10.1 (± 0.4)	10.0 (± 0.5)	1
SP+AM	94.1 (± 0.1)	93.4 (± 0.1)	92.6 (± 0.2)	92.3 (± 0.2)	85.4 (± 0.3)	2
SP+AM+AR	94.5 (± 0.0)	94.9 (± 0.0)	94.3 (± 0.0)	94.5 (± 0.0)	94.2 (± 0.0)	2
SP+AM+AR+Sens.	94.8 (± 0.0)	94.7 (± 0.0)	94.8 (± 0.0)	94.6 (± 0.0)	94.7 (± 0.0)	3

Table 11. Accuracy of 90% pruned ResNet-18 on CIFAR-10 when weights are perturbed by the PCM cells. Baseline accuracy after the pruning (when there is no noise) is 94.8%. SP: sign protection, AM: adaptive mapping, AR: sparsity-driven adaptive redundancy, Sens.: sensitivity-driven adaptive redundancy.

regarded as a promising compression method. In addition to compression, distillation has been shown to be an effective method for other desired NN attributes such as generalizab-

ility and adversarial robustness (Papernot et al., 2016). In this work, we define “robustness” as preserving a network’s downstream classification accuracy when noise is added

Neural Network Compression for Noisy Storage Devices

	Naive Training (no noise)	Robust Training (with N(0, 0.01))	Robust Training (with N(0, 0.006))	Additional Bits
No Noise	95.10	95.50	95.60	0
PCM Noise (No Protection)	9.70(± 1.0)	8.30 (± 0.4)	9.90 (± 1.1)	1
PCM Noise+SP	9.70(± 1.5)	10.63 (± 0.2)	10.33 (± 0.2)	2
PCM Noise+SP+AP	90.60(± 0.2)	94.73 (± 0.1)	94.80 (± 0.2)	2
PCM Noise+AP	27.69(± 8.2)	86.20 (± 0.4)	81.83 (± 4.2)	1
PCM Noise+AP+Sens	36.21(± 3.1)	86.73 (± 2.2)	78.93 (± 4.4)	2
PCM Noise+SP+AP+Sens	94.95(± 0.3)	95.03 (± 0.1)	95.03 (± 0.1)	3

Table 12. Accuracy of ResNet-18 on CIFAR-10 when weights are perturbed by the PCM cells. Baseline accuracy (when there is no noise at train or test time) is 95.10%. SP: sign protection, AP: adaptive protection (adaptive mapping+sparsity-driven adaptive redundancy), Sens.: sensitivity-driven adaptive redundancy. Experiments are conducted three times.

	Naive Training (no noise)	Robust Training (with N(0, 0.01))	Robust Training (with N(0, 0.006))	Additional Bits
No Noise	76.60	76.60	76.60	0
PCM Noise (No Protection)	0.001(± 0.0)	0.001 (± 0.0)	0.001 (± 0.0)	0
PCM Noise+SP	0.001(± 0.0)	0.004 (± 0.0)	0.002 (± 0.0)	1
PCM Noise+AP	0.001(± 0.0)	0.002 (± 0.0)	0.001 (± 0.0)	1
PCM Noise+SP+AP	66.00(± 0.8)	69.00 (± 0.3)	69.20 (± 0.2)	2
PCM Noise+AP+Sens	0.003(± 0.0)	0.006 (± 0.0)	0.005 (± 0.0)	2
PCM Noise+SP+AP+Sens	68.80 (± 0.3)	70.20 (± 0.0)	70.40 (± 0.1)	3

Table 13. Accuracy of ResNet-50 on ImageNet when weights are perturbed by the PCM cells. Baseline accuracy (when there is no noise at train or test time) is 74.4%. SP: sign protection, AP: adaptive protection (adaptive mapping+sparsity-driven adaptive redundancy), Sens.: sensitivity-driven adaptive redundancy. Experiments are conducted three times.

to the weights. This is achieved in part by robust training in the previous section where a trained network is robust to pruning and noise on the weights. Here, we present a novel student loss function that would make a (compressed) student network more robust to noise with no change in the teacher network training:

$$\mathcal{L}_s = (1 - \lambda)\mathbb{E}_{x,y \sim p_{data}}[-\log p_{g(\hat{w}_s)}(y|x)] + \lambda\mathbb{E}_x[D_{KL}(p_{w_t}(y|x)||p_{g(\hat{w}_s)}(y|x))]$$

In the experiments, we use a temperature parameter of $T = 1.5$ and equally weight the contributions of the student network’s cross entropy loss and the KL term ($\lambda = 0.5$). Similar to robust training, the noise level (standard deviation) during training is adjusted according to r and α values to be used at storage time. We give the full results on CIFAR-10 with confidence intervals in Tables 14 and 15 with weights perturbed by PCM cells and Gaussian noise, respectively. We also present the same set of experiments on MLP distilled from LeNet (on MNIST) in Tables 16 and 17. As in CIFAR-10 experiments, noise injection during distillation makes the student network more robust to both PCM and Gaussian noise in MNIST experiments.

Neural Network Compression for Noisy Storage Devices

	Number of PCM cells	Teacher ResNet-18	Teacher ResNet-20	Student ResNet-20	Noisy Student ResNet-20	Add. Bits
No Noise	16	95.70	92.50	92.90	93.00	0
PCM+AP	3	16.23 (\pm 1.6)	48.38 (\pm 14.3)	73.38 (\pm 2.4)	81.75 (\pm 1.5)	1
PCM+SP+AP	1	93.35 (\pm 0.5)	86.30 (\pm 1.5)	88.58 (\pm 0.4)	90.65 (\pm 0.7)	2
	3	94.78 (\pm 0.2)	89.73 (\pm 0.2)	89.98 (\pm 0.3)	91.33 (\pm 0.2)	
PCM+AP+Sens.	1	9.60(\pm 0.4)	29.68 (\pm 0.4)	38.18 (\pm 7.2)	69.49 (\pm 3.7)	2
PCM+SP+AP+Sens.	1	93.36 (\pm 0.2)	88.40 (\pm 1.4)	88.96 (\pm 0.7)	91.10 (\pm 0.3)	3
	3	94.90 (\pm 0.2)	89.92 (\pm 0.5)	90.44 (\pm 0.6)	91.78 (\pm 0.2)	

Table 14. Accuracy of ResNet-20 distilled from ResNet-18 on CIFAR-10 when weights are perturbed by the PCM cells. SP: sign protection, AP: adaptive protection (adaptive mapping+sparsity-driven adaptive redundancy), Sens.: sensitivity-driven adaptive redundancy. During the distillation of noisy student, a Gaussian noise with $N(0,0.01)$ is injected onto the weights. Experiments are conducted five times.

	Teacher ResNet-18	Teacher ResNet-20	Student ResNet-20	Noisy Student ResNet-18	Additional Bits
No Noise	95.70	92.50	92.90	93.00	0
$N(0,0.01)$ +No Protection	82.90 (\pm 2.3)	86.44 (\pm 1.6)	89.10 (\pm 0.7)	90.56 (\pm 0.4)	0
$N(0,0.01)$ +SP+AP	95.60 (\pm 0.0)	92.30 (\pm 0.1)	92.66 (\pm 0.0)	92.76 (\pm 0.1)	2
$N(0,0.02)$ +No Protection	10.88 (\pm 1.2)	45.36 (\pm 8.8)	65.50 (\pm 7.0)	77.78 (\pm 3.7)	0
$N(0,0.02)$ +SP+AP	95.70 (\pm 0.0)	91.68 (\pm 0.4)	92.30 (\pm 0.1)	92.36 (\pm 0.2)	2

Table 15. Accuracy of ResNet-20 distilled from ResNet-18 on CIFAR-10 when weights are perturbed by the Gaussian noise. SP: sign protection, AP: adaptive protection (adaptive mapping+sparsity-driven adaptive redundancy). During the distillation of noisy student, a Gaussian noise with $N(0,0.01)$ is injected onto the weights. Experiments are conducted five times.

	Teacher LeNet	Teacher MLP (Student baseline)	Student MLP (No Noise)	Noisy Student MLP (with $N(0,0.1)$)	Noisy Student MLP (with $N(0,0.006)$)	Number of PCM cells	Additional Bits
No Noise	99.20	97.50	97.80	96.30	97.30	16	0
PCM+SP	98.94 (\pm 0.0)	91.86 (\pm 1.7)	87.46 (\pm 3.7)	95.46 (\pm 0.1)	93.12 (\pm 1.4)	1	1
PCM+AP	98.60 (\pm 0.2)	92.76 (\pm 1.6)	95.40 (\pm 1.0)	95.78(\pm 0.2)	96.04 (\pm 0.4)	1	1
PCM+SP+AP	99.20 (\pm 0.0)	97.04 (\pm 0.1)	97.46 (\pm 0.2)	96.12 (\pm 0.1)	97.58 (\pm 0.1)	1	2
PCM+AP+Sens.	98.88 (\pm 0.1)	95.04 (\pm 0.5)	97.10 (\pm 0.1)	95.92(\pm 0.1)	97.46 (\pm 0.1)	1	2
PCM+SP+AP+Sens.	99.20 (\pm 0.0)	97.20 (\pm 0.0)	97.72 (\pm 0.1)	96.14(\pm 0.1)	97.80 (\pm 0.1)	1	3

Table 16. Accuracy of MLP distilled from LeNet on MNIST when weights are perturbed by the PCM cells. SP: sign protection, AP: adaptive protection (adaptive mapping+sparsity-driven adaptive redundancy), Sens.: sensitivity-driven adaptive redundancy. Experiments are conducted five times.

	Teacher LeNet	Teacher MLP (Student baseline)	Student MLP (No Noise)	Noisy Student MLP (with $N(0,0.1)$)	Noisy Student MLP (with $N(0,0.006)$)	Additional Bits
No Noise	99.20	97.50	97.80	96.30	97.30	0
$N(0,0.1)$ +No Protection	22.60 (\pm 7.7)	77.72 (\pm 3.8)	58.90 (\pm 3.6)	93.80 (\pm 0.4)	62.20 (\pm 3.5)	0
$N(0,0.1)$ +SP+AP	99.22 (\pm 0.0)	95.92 (\pm 0.3)	95.96 (\pm 0.8)	95.82 (\pm 0.2)	97.02 (\pm 0.2)	2
$N(0,0.2)$ +No Protection	12.02 (\pm 3.0)	33.50 (\pm 3.4)	24.78 (\pm 6.3)	74.82 (\pm 5.0)	25.02 (\pm 2.8)	0
$N(0,0.2)$ +SP+AP	99.18 (\pm 0.1)	90.36 (\pm 1.0)	86.30 (\pm 4.6)	95.06 (\pm 0.3)	93.06 (\pm 2.1)	2
$N(0,0.06)$ +No Protection	99.24 (\pm 0.0)	97.38 (\pm 0.1)	97.82 (\pm 0.1)	96.28 (\pm 0.0)	97.86 (\pm 0.0)	0
$N(0,0.06)$ +SP+AP	99.20 (\pm 0.0)	97.50 (\pm 0.0)	97.80 (\pm 0.0)	96.30 (\pm 0.0)	97.90 (\pm 0.0)	2

Table 17. Accuracy of MLP distilled from LeNet on MNIST when weights are perturbed by the Gaussian noise. SP: sign protection, AP: adaptive protection (adaptive mapping+sparsity-driven adaptive redundancy). Experiments are conducted five times.

E.5. LOGISTIC REGRESSION EXPERIMENTS

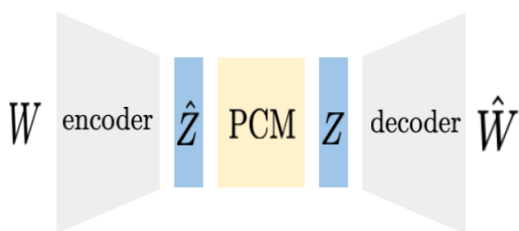
The logistic regression experiments are conducted in two steps. First, we train a logistic regression model on each Gaussian mixture dataset – recall that there are 50 datasets per “easy” (separated means) and “hard” (overlapping means) tasks. For learning the classifier, we use a batch size of 128 and train each model with SGD, where the learning rate = 0.1 and weight decay = 0.0005. We perform early stopping for each model on a held-out validation set.

After training the logistic regression models, we use an autoencoder with both MLP encoder and decoder architectures and ReLU nonlinearities, as shown in Table 18. The autoencoder for both the “easy” and “hard” tasks is trained for 10 epochs with a batch size of 100 using the Adam optimizer with learning rate = 0.001, $\beta_1 = 0.9$, $\beta_2 = 0.999$, and early stopping on a held-out validation set.

We test the autoencoder on both Gaussian and PCM noise: that is, we corrupt the 1-dimensional encoder output (z-representation of the classifier weights) with the appropriate perturbation before passing in the encoded representation into the decoder. Figure 7 provides an illustration of the autoencoding process for the PCM array, which is analogous to the Gaussian noise setup.

Name	Component
(Encoder) Input Layer	Linear $3 \rightarrow 1$, ReLU
(Encoder) Hidden Layer	Linear $1 \rightarrow 1$
(Decoder) Hidden Layer	Linear $1 \rightarrow 1$, ReLU
(Decoder) Output Layer	Linear $1 \rightarrow 3$

Table 18. MLP-based autoencoder architecture for synthetic experiments, trained on 50 logistic regression classifiers per task.



(a) Autoencoder for logistic regression experiment.

Figure 7. Illustration of the autoencoder framework used for the logistic regression experiments. The input weight W is mapped to a compressed representation \hat{Z} by an encoder module, which is then perturbed by the PCM (or analogously, Gaussian) noise channel to become a perturbed representation Z . This perturbed representation is then passed to the decoder, which produces a reconstructed weight \hat{W} .

In Figures 8 and 9, we qualitatively analyze the learned representations of the logistic regression classifier weights. In

Figure 8(a), we plot all 50 datasets of the Gaussian mixtures (“easy task”) as well as the true decision boundaries for each of the 50 logistic regression models, each boundary colored by the magnitude of its z-representation as learned by the autoencoder. We plot the same for the “hard task” in Figure 8(b). For the easy task, we note that the classifiers are encoded by their relative location in input-space: those that are in the lower left corner of the scatter plot have smaller magnitudes than those on the upper right. For the hard task, however, the z-representations appear to be fairly random – at a first glance, there does not appear to be a particular correlation between the magnitudes of the z-encodings and the original classifier weights.

We further explore this phenomenon for the hard task in Figure 9. For two particular datasets (though the trend holds across all 50 datasets), we color the original data points by their mixture component as well as the true decision boundary by the magnitude of its z-encoding. As shown in Figure 9(a) and (b), we find that the autoencoder has learned to map all classifiers with the positive class to the left of the decision boundary to z-representations with large magnitude; conversely, those with the positive class to the right of the decision boundary are encoded to z-representations with smaller magnitudes. Through this preliminary investigation, we demonstrate that the end-to-end approach for learning both the compression scheme while taking the physical constraints of the storage device into account shows promise.

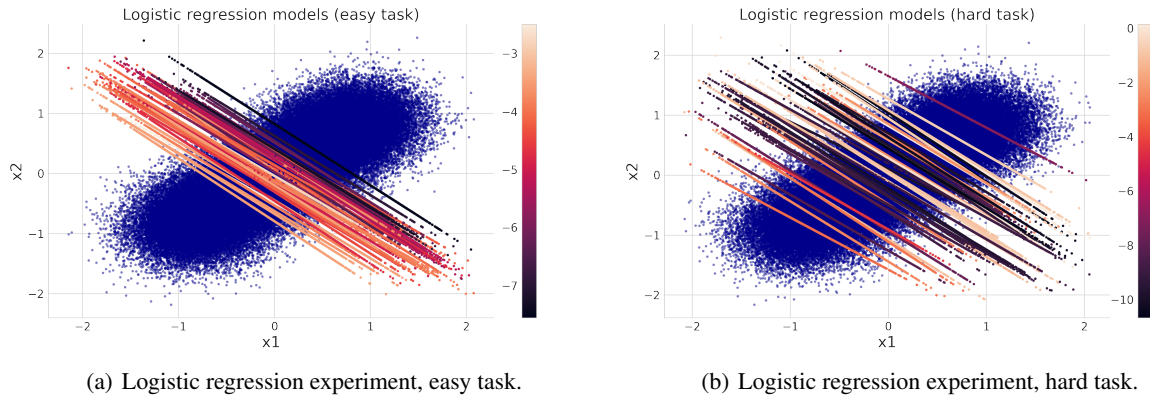


Figure 8. Qualitative visualizations of the learned representations in the logistic regression experiment. (a) shows all 50 datasets with the true decision boundaries colored by the magnitude of their z-representations for the “easy task”, while (b) shows the analogous plot for the harder task with overlapping means.

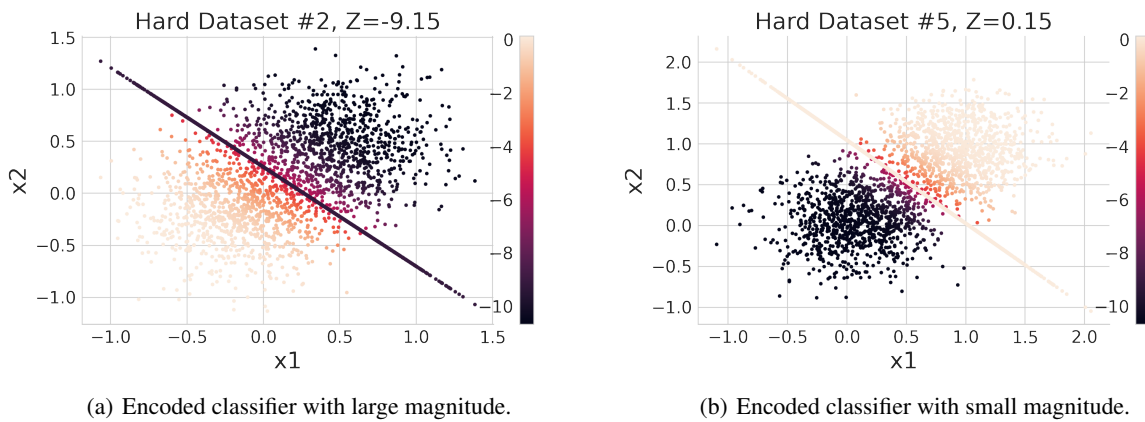


Figure 9. Qualitative visualizations of the learned representations for the hard logistic regression task. We find in (a) that classifiers with large magnitudes in z-space have the positive labels to the left of the decision boundary, while (b) those with small magnitudes have the positive labels to the right of the decision boundary.